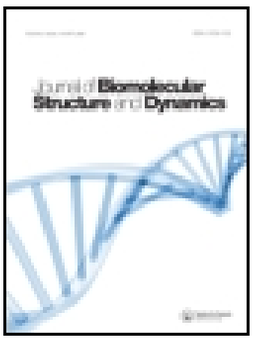

Taylor & Francis
Taylor & Francis Group

Journal of Biomolecular Structure and Dynamics

ISSN: (Print) (Online) Journal homepage: https://www.tandfonline.com/loi/tbsd20

Identification of potent EGFR-TKD inhibitors from NPACT database through combined computational approaches

Showkat Ahmad Mir, Auwal Muhammad, Archana Padhiary, Nirius Jenen Ekka, Iswar Baitharu, Pradeep Kumar Naik & Binata Nayak

To cite this article: Showkat Ahmad Mir, Auwal Muhammad, Archana Padhiary, Nirius Jenen Ekka, Iswar Baitharu, Pradeep Kumar Naik & Binata Nayak (2023): Identification of potent EGFR-TKD inhibitors from NPACT database through combined computational approaches, Journal of Biomolecular Structure and Dynamics, DOI: 10.1080/07391102.2023.2171133

To link to this article: https://doi.org/10.1080/07391102.2023.2171133

JOURNAL OF BIOMOLECULAR STRUCTURE AND DYNAMICS
https://doi.org/10.1080/07391102.2023.2171133

Identification of potent EGFR-TKD inhibitors from NPACT database through combined computational approaches

Showkat Ahmad Mir[a], Auwal Muhammad[b], Archana Padhiary[a], Nirius Jenen Ekka[a], Iswar Baitharu[c], Pradeep Kumar Naik[d] and Binata Nayak[a]

[a]School of Life Sciences, Sambalpur University, Jyoti Vihar, Odisha, India; [b]Department of Physics, Kano University of Science and Technology, Wudil, Nigeria; [c]Department of Environmental Sciences, Sambalpur University, Jyoti Vihar, Odisha, India; [d]Department of Biotechnology and Bioinformatics, Sambalpur University, Jyoti Vihar, Odisha, India

Communicated by Ramaswamy H. Sarma

ABSTRACT

Cancer is the world's second leading cause of death, and there are no approved herbal therapies. The epidermal growth factor receptor tyrosine kinase (EGFR-TK) receptor is a transmembrane protein with eight domains that is found in almost every cancer type and plays an important role in abnormal cell cellular function and causes malignant outcomes. The current study aimed to virtually screen phytochemicals from the NPACT database against EGFR-TKD and also to identify potential inhibitors of this transmembrane protein among plant candidates for anticancer drug development. The docking scores of the chosen phytochemicals were compared with the control (erlotinib). Kurarinone, (2S)-2-methoxykurarnione, and Sophoraflavanone-G exhibited a stronger binding affinity of −18.102 kcal/mol, −14.243 kcal/mol, and −13.759 kcal/mol than erlotinib −12.783 kcal/mol. Moreover, several online search engines were used to predict ADME and toxicity. The drug-likeness of selected phytochemicals was higher than the reference (erlotinib). A 100 ns molecular dynamic (MD) simulation was also applied to the docked conformations to examine the stability and molecular mechanics of protein-ligand interactions. Furthermore, the calculated molecular mechanics Poisson Boltzmann surface area energy of (2S)-2-methoxykurarnione was found to be −129.555 ± 0.512 kJ/mol, which approximately corresponds to the free energy of the reference molecule −130.595 ± 0.908 kJ/mol. We identify phytoconstituents present in Sophora flavescens from the NPACT database, providing key insights into tyrosine kinase inhibition and may serve as better chemotherapeutic agents. Experimental validation is required to determine the anti-EGFR potency of the potent lead molecules discussed in this study.

ARTICLE HISTORY
Received 29 September 2022
Accepted 27 December 2022

KEYWORDS
Phytochemicals; ADMET; molecular docking; molecular dynamics simulations; MM-PBSA

1. Introduction

Cancer is the second most deadly disease globally. In 2022, 1.9 million new cases and 609,360 numbers of deaths were reported only in the United States (ACS, 2022). Among all cancers, breast and lung cancer is the leading cause of mortality. Cancer can be prevented by using various therapies such as radiation therapy proton beam therapy, three-dimensional conformal radiation therapy, and chemotherapy (Xu et al., 2017; Mori et al., 2020; Levin et al., 2005). However, treating patients with these therapies cause multiple side effects which may stumble the expectancy of life. Receptor tyrosine kinases (RTKs) including VEGF, EGFR, EGFR-VIII, HER-II, HER-III, IGFR, c-Met, PDGFR, FGFR, AXL, and IL-6R play a crucial role in cellular signaling among abnormal cells (Fantl et al., 1993). These receptors are transmembrane proteins consisting of ectodomain and endodomain. The ectodomain comprises 4 domains (I, II, III, and IV) and the endodomain is a kinase domain known as the cytoplasmic domain. Besides these two domains, the fourth domain of the ectodomain is connected with the transmembrane domain followed by juxtamembrane and connects cytoplasmic domain thus forming a complete epidermal growth factor receptor tyrosine kinase (EGFR-TKD) transmembrane domain (Garrett et al., 2002; Ogiso et al., 2002). Apart from EGFR-TKD, Ras protein and S-Adenosyl-l-methionine (SAM III) are targeted because Ras protein mutation-mediated activity has been found in cancer patients on a regular basis (Chen et al., 2021; Chen et al., 2022).

In almost all types of cancer cells, the RTKs are present to initiate the downstream signaling upon binding of a ligand (such as EGF, TGF, HGF), to the ectodomain of EGFR. During ligand bindings, the EGFRs dimerize and activate auto-phosphorylations of the cytoplasmic domain thus activating the tyrosine-dependent enzymes SOS, JAK, RAF, RAS, SRC, STAT, etc., that are the key enzymes to regulate differentiation, growth, survival proliferation, mortality and, angiogenesis (Jeppe Knudsen et al., 2014; Xia et al., 2018), inhibiting the function of the RTKs prevents abnormal cell growth (Shimizu et al., 2008; Shimizu et al., 2011).

CONTACT Showkat Ahmad Mir showkat@suniv.ac.in School of Life Sciences, Sambalpur University, Jyoti Vihar, Odisha768019, India; Binata Nayak binatanayak@suniv.ac.in School of Life Sciences, Sambalpur University, Jyoti Vihar, Odisha768019, India.

Supplemental data for this article can be accessed online at https://doi.org/10.1080/07391102.2023.2171133.

Multiple synthetic drugs were rationale designed to inhibit the function of RTK including erlotinib, gefitinib, osemertinib, and sunitinib which accommodate themselves in the binding pocket. Over the last five years, substantial tyrosine kinase inhibitors (TKIs) have been authorized for a variety of cancers. These compounds block kinase enzymes, which operate as 'on' or 'off' switches in a variety of cellular processes such as proliferation, apoptosis, metabolism, and transcription. Rash, mucositis, and diarrhea are all frequent side effects of EGFR TKIs (Melosky & Hirsh, 2014).

The rash is one of the most prevalent side effects seen in people using EGFR inhibitors. The approval of afatinib in non-small-cell lung cancer (NSCLC) revealed that 89 percent of patients treated with the drug had a rash. Other prevalent side effects are diarrhea (in 95% of patients), stomatitis (72%), paronychia (57%), and dry skin (29%) (Oliveira, 2015). Many inhibitors of EGFR-TKD have toxicity risks. Malformations are also reported by using imatinib among normal delivery pregnancy patients (Pye et al., 2008), and erlotinib itself shows hepatotoxicity. Patients treated with tyrosine kinase inhibitors showed mild to moderate toxicity. But due to the adverse effects (AEs) of TKIs, the treated dose was reduced to a small proportion and can improve the quality of the life (Ding et al., 2017;). The side effects include dermatological responses, hepatoxicity, stomatitis, interstitial lung diseases, and eye toxicity (Shah & Shah, 2019). However, discontinuing tyrosine kinase inhibitors (TKIs) before patients develop severe adverse effects such as hepatotoxicity, improves the performance of the drug among patients with positive EGFR-mutated tumors (Sakata et al., 2020). As the adverse effects on patients from these drugs are a major issue in the present scenario, alternative Phytochemicals have a wide history in Ayurveda. Combating the hurdles occurring due to synthetic drug molecules, phytochemicals are a good option to serve as chemotherapeutics and inhibit the cellular function of abnormal cells with no side effects. In this present study, we explore some phytochemicals from the Naturally Occurring Plant-based Anticancerous Compound Activity Target (NPACT) database that may serve as better anti-EGFR-TKD agents. Thus, an *in silico* approaches and various search engines were used to determine the efficacy of the phytochemicals from the selected database against EGFR.

2. Methodology

2.1. Retrieval of target protein and binding site prediction

The wild-type EGFR-TKD X-ray crystallographic structure 1M17 (Stamos et al., 2002) was searched and obtained from the online database www.rcbs.com. Structural analysis of tyrosine kinase domain was done by using the https://www.ncbi.nlm.nih.gov/Structure/icn3d web server (Wang et al., 2020).

The occupancy of the amino acids existed in the binding site was found in the C-lobe and N-lobe of tyrosine kinase domain. The 3 D X-ray crystallographic structure 1M17 were used to identify the binding site of TKD, using ArgusLab software () and amino acids existing in the active site of the TKD (1m17.pdb) were found to be Leu694, Ala719, Lys721, Glu738, Leu764, Thr766, Gln767 Leu768, Met769, Pro770, Phe771, Gly772, Leu820, Thr830, and Asp831.

2.2. Ligand properties and molecular docking assessment

The Naturally Occurring Plant-based Anti-cancerous Compound Activity Target Database was screened with the aimed to identify the non-toxic drug-like molecule using online servers such as pKCSM, and Swiss ADME, MolSoft L.L.C (Pires et al., 2015; Daina et al., 2017). The 2 D structures were converted to a Simplified Line Entry System (SMILES) by using open babel (O'Boyle et al., 2011). Furthermore, the non-toxic molecules were screened for drug-likeness scores using the MolSoft L.L.C server (Molsoft, 2007). Out of 1800 molecules, some molecules showed non-toxic behavior and higher drug-likeness score (Table S1). These non-toxic molecules were further implemented for molecular docking simulation to observe the hits with the binding site of the EGFR-TKD. The phytochemical database contains 1800 molecules and erlotinib was taken as a reference. All phytochemicals were prepared by using the MMFF94x force field in MOE09 software. The structure was minimized in a vacuum for 1 ns using the GROMOS96 force field. The final minimized structure was obtained for further molecular investigations. The protein was prepared, water molecules were removed, and hydrogen was incorporated, partial charges were added to the system by using 3 D protonate application of MOE09 software. Virtual screening was carried out using the London dG method, placement Triangle Matcher. Retain module was dropdown to 10, and final refined poses was ranked by the MM/GBVI binding free estimation. The data generated were written in output database after the docking is finished. Finally, LigX module was used to determine the interactions exhibited by phytochemicals with the catalytical site of the tyrosine kinase.

Table 1. Molecular docking of Kurarinone, (2S)-2-Methoxykurarinone, Sophoraflavanone, and Erlotinib with the template protein EGFR-TKD and the observed interactions were found with the key amino acids residues in the binding site.

Ligand	Receptor	Residue	Chain	Type	Score	Distance
1. Kurarinone						
H 4793	OD 2582	ASP 831	1M17	H-don	84.3%	1.22
O 4747	NZ 805	LYS 721	1M17	H-acc	14.4%	3.17
O 4746	OG 1500	THR 766	1M17	H-acc	73.3%	2.80
2. (2S)-2-Methoxykurarinone						
O 4747	OG 1500	THR 766	1M17	H-don	17.7%	3.00
H 4809	O 2325	ARG 817	1M17	H-don	48.3%	1.42
O 4747	OG 1500	THR 766	1M17	H-acc	17.7%	3.00
O 4746	N 1544	MET 769	1M17	H-acc	16.6%	3.10
3. Sophoraflavanone-G						
O 4748	OG 1500	THR 766	1M17	H-don	90.2%	2.43
H 4802	OD 2582	ASP 831	1M17	H-don	41.7%	1.33
O 4747	OG 1500	THR 766	1M17	H-acc	22.1%	2.94
O 4748	OG 1500	THR 766	1M17	H-acc	90.2%	2.43
O 4746	N 1544	MET 769	1M17	H-acc	77.5%	2.74
4. Erlotinib						
N 4787	N 1544	MET 769	1M17	H-acc	22.6%	3.15

2.3. DFT assessment of lead phytochemicals

The lead phytochemicals obtained from the NPACT database by *in-silico* prediction were subjected to molecular orbital calculations by applying the Density Functional Theory (DFT) method. The DFT calculations were carried out by setting up a correlation function (B3LYP) and basis set 6-31 + G* level. Higher occupied and lower unoccupied atomic orbitals were identified. The frontal orbitals HOMO and LUMO were calculated from those orbitals the energy gap (ΔE) was determined finally other QM parameters were calculated such as ionization potential (I) I =-E_{HOMO} (eV), softness (σ) $\sigma = 1/\eta$, chemical potential (μ) μ=-I + A/2, electronegativity (χ) χ= I + A/2, hardness (η) η = I-A/2, electron affinity A=-E_{LUMO} (eV) and global electrophilicity (ω) $\omega = \mu 2/2\eta$ were calculated (Parr et al., 1999; Mebi, 2011) by the mentioned descriptors.

2.4. Molecular dynamic simulations and molecular mechanics Poisson Boltzmann surface area (MM-PBSA) assessments

The molecular dynamic simulations were carried out by using the gromacs 5.1.1 (Jo et al., 2008; Pereira et al., 2019). The protein (TKD) was prepared by passing through multiple steps. The structure was cleaned, and the inhibitor was removed from the protein-ligand complex and generate topology using AMBER99SB-ILDN.ff (Wang et al., 2006; Lindorff-Larsen et al., 2010) with recommended TIP 3-point model. The ligand topology was generated using t-leap and parameters were assigned using GAFF (Sousa da Silva & Vranken, 2012; Kashefolgheta & Verde, 2017). Next, the complex was placed in the grid box which is 1 nm apart from the periodic boundaries. The system was solvated and neutralized by using Na^+ and Cl^-. The steepest descent method was used for energy minimizations. The temperature and pressure were adjusted to 300 K at 1 bar using a thermostat and barostat coupling constants. The coulomb's cut-off scheme was kept at 1.2 nm and long-range electrostatic interactions were handled by the PME algorithm. To constrain bond length, the LINICS algorithm was used (Borkotoky & Murali, 2018; Hess et al., 1997). The NVT and NPT methods were used to equilibrate the system for 100 ps (Brooks et al., 2009). The simulations were performed by applying a time step of 2 fs for 100 ns. The RMSD, RMSF, Hbond distance, RMSF modules of gromacs were used for MDS analysis

2.5. Assessment of free binding energy (MM-PBSA)

Free energy was calculated by linearized traditional PBE methods. Multiple Debye-Huckle sphere boundary conditions and ionic strength of 0.150 M concentrations were used. The values of dielectric constants of protein and water considered for implicit solvation were set to 4 and 80 respectively, while default grid dimensions of x = 129, y = 129, and z = 97 Å was maintain. Nonpolar solvation energy was calculated using solvent accessible surface area (SASA) model. Also, the default values of surface tension of the solvent, and SASA energy constant from previous MM/PBSA calculations of 0.0226778 kJ/mol $Å^2$, and 3.84982 kJ/mol were used respectively (Ayoub et al., 2019).

The average free energy binding of non-toxic phytochemicals and erlotinib-bound EGFR-TKD complexes was performed by using *g_mmpbsa* (Kumari et al., 2014). The final 2000 frames from input files were obtained after the completion of molecular dynamic simulations and were used for free energy binding calculations. The average free energy binding was calculated by the bootstrap method using MmPbSaStat.py. The decomposition energy of each amino acid contributes to free energy bindings was calculated by the MnPbDecomp.py module of *g_mmpbsa*. The ΔG_{bind} was calculated according to the following equation.

$$\Delta G_{binding} = \Delta G_{complex} - \Delta G_{protein} + \Delta G_{ligand} \quad \text{(i)}$$

$G_{complex}$ denotes the total free energy of the protein-ligand complex, whereas the isolated total free energy of protein and ligand are represented as $G_{protein}$ and G_{ligand} in the above-given equation.

The free energy of an individual entity is summed up by the equation given below:

$$G_x = E_{MM} - TS + G_{Solvation} \quad \text{(ii)}$$

The protein-ligand complex is denoted by X, and EMM denotes an average molecular mechanic's potential energy in a vacuum, as calculated by equation (ii).

Gsolvation denotes the free energy of solvation, TS denotes the entropic free energy contribution in a vacuum, and T denotes temperature and S entropy. For MD studies of complexes with single trajectory approaches, the entropy term is negligible as its inclusion does not improve the agreement with the experiment (Muhammad et al., 2020; Yang et al., 2011).

$$E_{MM} = E_{bonded} + E_{nonbonded} = E_{bonded} + E_{vdW} + E_{elec} \quad \text{(iii)}$$

Ebonded represents the collective interactions of the dihedral, angle, and bond. whereas the nonbonded interactions consist of van der Waals (E_{vdW}) and electrostatic (E_{elec}) interactions.

Furthermore, Free Energy of Solvation, Polar Solvation Energy, Non-polar Solvation Energy, SASA-Only, and polar models were calculated. The decomposed contributions of the free energy binding of each amino acid are calculated from ΔE_{MM}, ΔG_{polar}, and $\Delta G_{nonpolar}$.

2.6. Principal component analysis and free energy landscape analysis

The movement of amino acids to a set of linearly uncorrelated variables is commonly studied using the principal component (PCA) analysis of statistics (Aier et al., 2016, Mir & Nayak, 2022). To begin with, the covariance matrix and eigenvalues were built using the Gromacs package gmx anaeig. By diagonalizing the covariance matrix, the eigenvectors are calculated. The associated motions in a sampled system were computed by using the gmx covar module. The graphs were plotted using the free Xmgrace software available on (http://plasma-gate.weizmann.ac.il/Grace/).

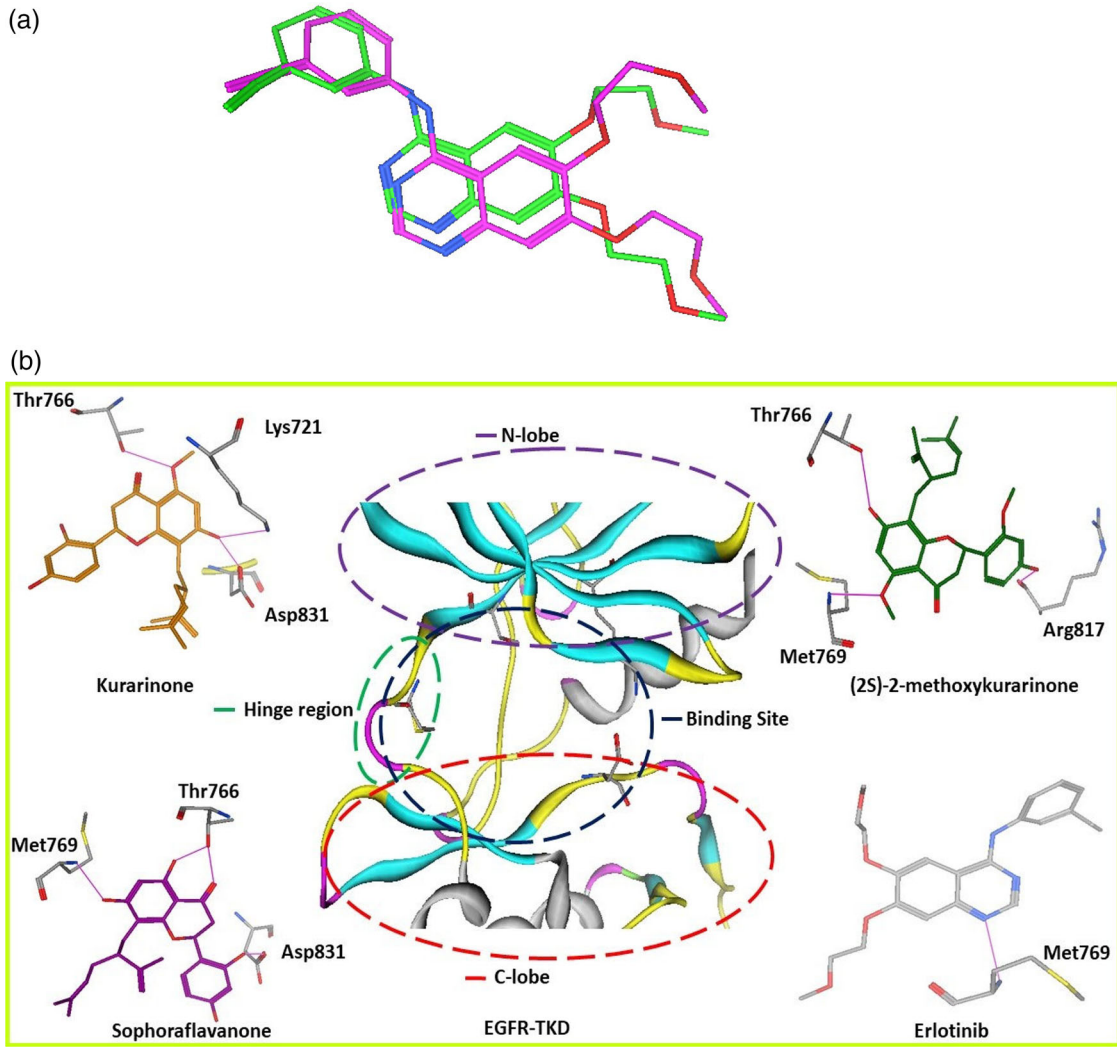

Figure 1. (a) The representation of the redocked erlotinib drug molecule with the experimental complex. The green color erlotinib was redocked as the control molecule and the pink carbon color erlotinib is complexed in the tyrosine kinase (1m17). (b) Phytochemicals achieved interactions with the key amino acids in the binding site of the EGFR-TKD. The N-lobe, C-lobe, hinge region, and the binding site was marked by dashed circles in blue in the middle figure which represents the binding site occupying the amino acids from N-lobe, C-lobe, and the hinge region.

3. Results and discussion

3.1. Molecular docking simulations

Molecular docking simulations are very useful tools to predict the ligand binding with the respective receptor and are used in both industrial and academic sectors. Molecular dockings were carried out using molecular operating environment (MOE-09) software. The docking method was validated by identifying the RMSD of the control molecule using the original experimental complex (1M17) and redocked in the binding site through which the RMSD was calculated and the value was found to be 1.3956 Å (Figure 1a). The NPACT database was screened with the (EGFR-TK) and the hits were observed with the binding site of the tyrosine kinase (TK). The top hits exhibited by the ligands were found to be with key amino acids MET 769, LYS721, ARG 817, and ASP831 in the catalytical site. Interestingly, Sophoraflavanone and (2S)-2-methoxykurarinone showed interactions with Met769 at the hinge region of the catalytical site. The Kurarinone did not show interactions with the Met769 but with other amino acids in the binding site, the interactions were found with better binding affinity. The 2-(2,4-Dihydrophenyl)-7-hydroxy-5-methoxy-8-(5-methyl-2-prop-1-en-2-ylhex-4-enyl)-2,3-dihydrochromen-4-one (Kurarinone) in which the 7-hydroxy and 5-methoxy groups of dihydrochromen-4-one showed robust bindings with sidechain OH group of Thr766, NH3 of Lys721, and COOH group of the Asp831.

Also, the (2S)-2-(2S)-7-hydroxy-2-(4-hydroxy-2-methoxyphenyl)-5-methoxy-8-[(2R)-5-methyl-2-prop-1-en-2ylhex-4enyl]-2,3-dihydrochromen-4-one ((2S)-2-methoxykurarinone) in which 7-hydroxy-5-methoxy dihydrochromen-4-one exhibited interactions with sidechain OH group of Thr766 and with Met769 NZ backbone atom also the 2-(2,4-Dihydroxyphenyl) exhibited interactions with amino acid Arg 817 COOH side chain group. Furthermore, the (Sophoraflavanone) (2S)-2-(2,4-dihydroxyphenyl)-5,7-dihydroxy-8-[(2R)-5-methyl-2-prop-1-en-2-ylhex-4-enyl]-2,3-dihydrochromen-4-one exhibited interaction with Thr766 and Met769 and Asp831 through 2,4-dihydroxyphenyl moiety and 5,7-dihydroxy 2,3-dihydrochromen-4-one.

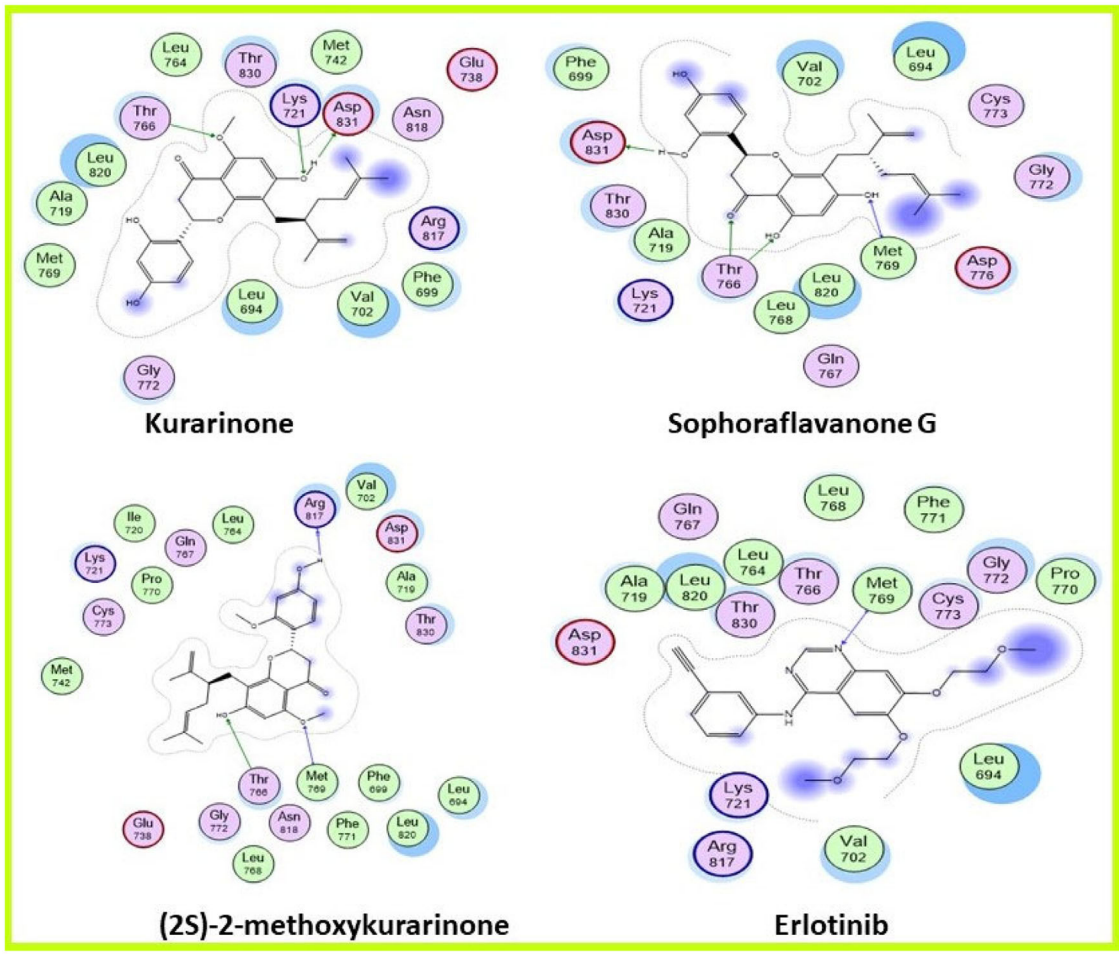

Figure 2. The 2 D interactions of respective phytochemicals with the binding site, phytochemicals exhibited similar interactions as reference molecule erlotinib. Kurarinone, Sophoraflavanone, and (2S)-2-methoxykurarinone showed interactions with Lys721, Thr766, Met769, Arg817, and Asp831 in the catalytical site including the hinge region of the tyrosine kinase.

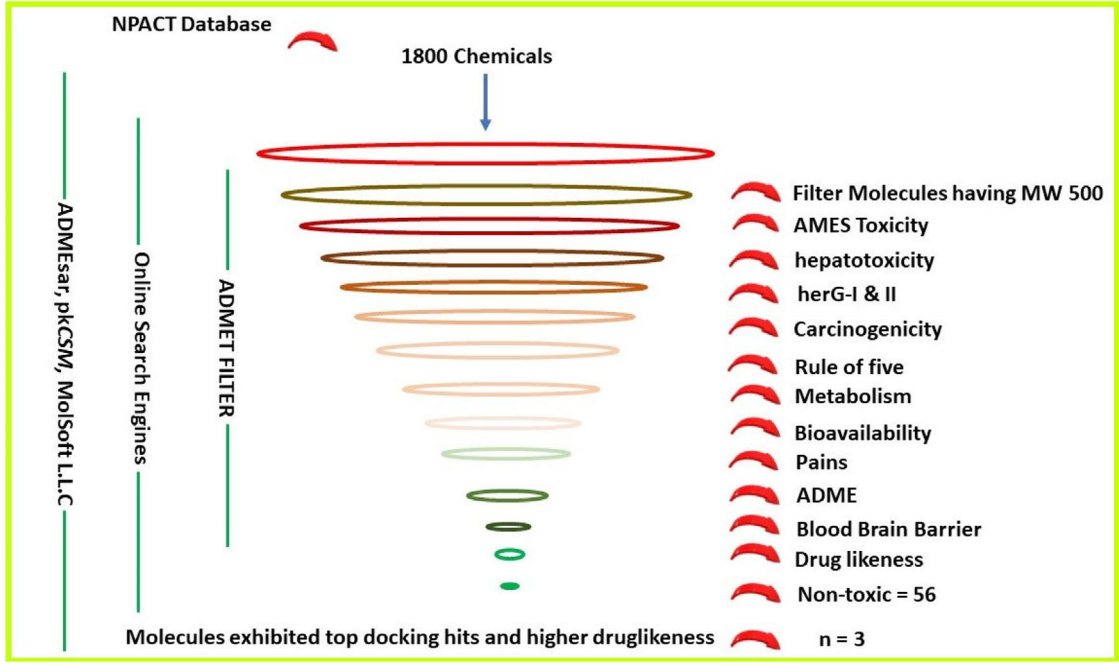

Figure 3. Identification of lead molecules from the phytochemical database using online search engines and found three phytochemicals, Kurarinone, (2S)-2-methoxykurarinone, and Sophoraflavanone-G.

Table 2. Global electrophilicity and associated terms, calculated by density functional theory using the B3LYP 6-31 + G* method.

Global Electrophilicity Parameters	Kurarinone	(2S)-2-methoxykurarinone	Sophoraflavanone G	Erlotinib
EHOMO (eV)	−5.888	−5.847	−6.112	−5.068
ELUMO (eV)	−1.237	−1.176	−1.912	−2.845
E gap (eV)	4.651	4.671	4.199	2.222
I =-EHOMO (eV)	5.888	5.847	6.111	5.068
μ=-I + A/2	−3.562	−3.511	−4.012	−3.957
A=-ELUMO (eV)	1.236	1.176	1.911	2.845
χ= I + A/2	3.562	3.511	4.012	3.957
η = I-A/2	2.325	2.335	2.099	1.111
σ =1/η	0.430	0.428	0.476	0.900
ω = μ2/2η	2.729	2.639	3.832	7.041

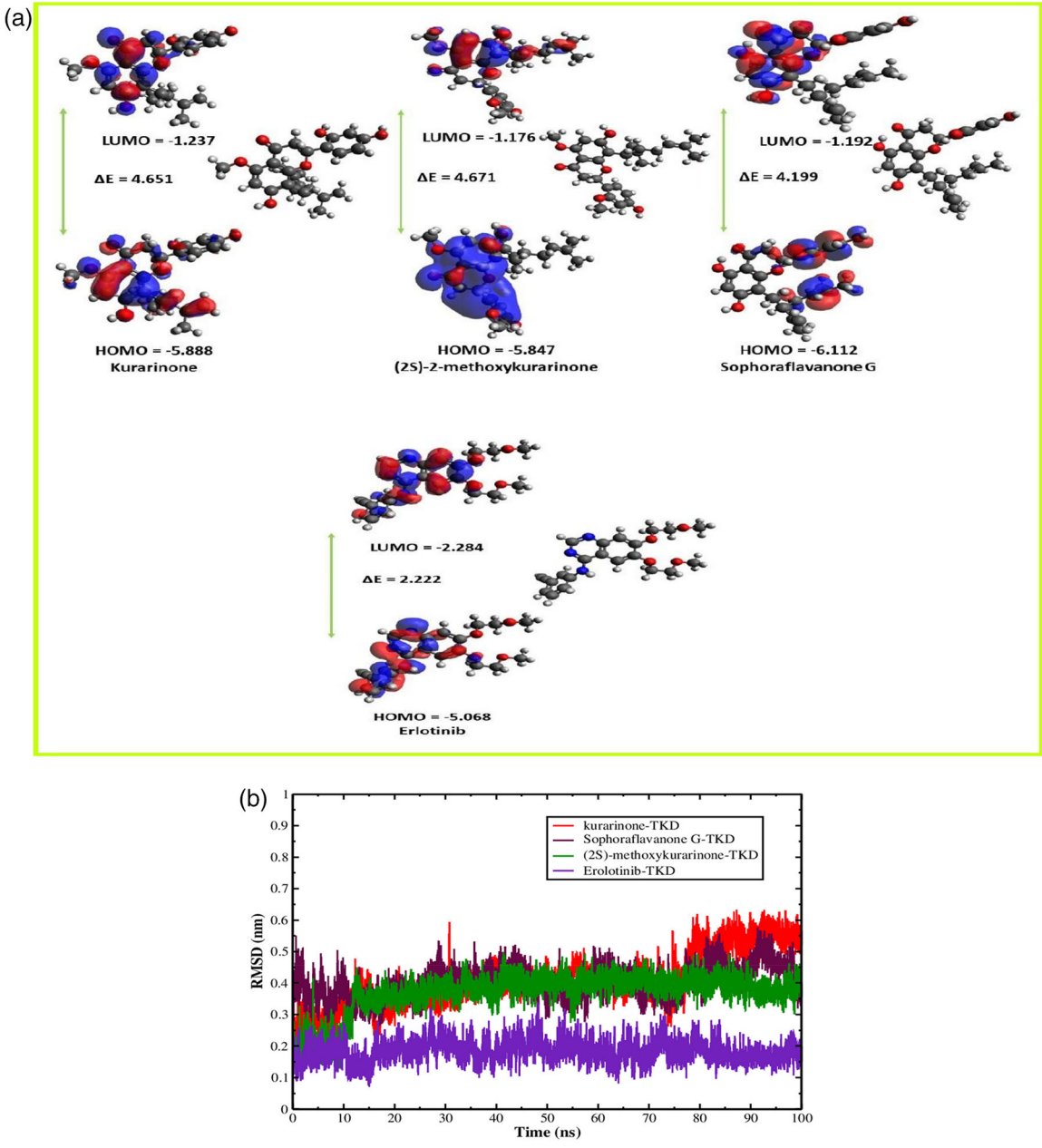

Figure 4. (a) The higher occupied molecular orbital (HOMO), lower unoccupied molecular orbitals (LUMO), and energy gap (ΔE) of the potent EGFR-TKD inhibitors Kurarinone, (2S)-2-methoxykurarinone, Sophoraflavanone G, and erlotinib were calculated. (b) RMSD plots of ligand Kurarinone, (2S)-2-methoxykurarinone, Sophoraflavanone-G, and erlotinib when superposed on TK and trajectories were achieved. Each complex is represented by the colors given in the legend box.

The hydrogen bonds of each amino acid take part in the interactions as well as the hydrogen bonds of ligands were removed for clear visualizations and orientations in the binding site of tyrosine kinase (Figures 1a, 1b, & 2).

The binding affinity of the selected phytochemicals Kurarinone, (2S)-2-methoxykurarinone, Sophoraflavanone, and Erlotinib were found to be −18.102 Kcal/mol, −14.243 Kcal/mol, −13.759 Kcal/mol, and −12.783 Kcal/mol

respectively (Table S1). The interactions exhibited by the ligand with the template protein EGFR-TKD were represented in Table 1 and the associated parameters such as interacted moieties of Kurarinone, (2S)-2-methoxykurarione, Sophoraflavanone-G and Erlotinib with EGFR-TKD, residues involved in interactions, type of bonding, docking score and distance of bonds in Å. The lead phytochemicals (2S)-2-methoxykurarione, and Sophoraflavanone-G showed similar interactions like erlotinib, and the interactions were found with key amino acid MET 769 those interactions find support from the several studied (Stamos et al., 2002, Mir et al., 2022). The amino acids surrounding to the molecules were represented in elemental color also Kurarinone, (2S)-2-methoxykurarione, Sophoraflavanone-G, and Erlotinib were colored in orange, green, marron, and elemental. The docking results showed that all three phytochemicals achieved higher binding affinity than reference molecule erlotinib against TKD (Table S1). These preliminary in-silico investigations demonstrated that present chosen phytochemicals interacted with key amino acid residues and accommodated in a binding pocket thus may serve as a potent inhibitor of the TK. Further investigations such as molecular dynamics simulations and MM-PBSA calculations are necessary to validate the docking study.

3.2. ADMET analysis

The Pharmacokinetic properties of 1800 molecules were investigated using online search engines SwissADME and pkCSM and MolSoft L.L.C. Potential drug-like candidates were filtered at early stages and selected molecules were chosen which are non-toxic and followed ADMET properties. This method is cost-effective, reliable, and reduces experimental costs. We assessed the ADMET filter of the NPACT database and remove molecules that are highly toxic such as AMES toxic, hepatotoxic, Ether go-to-go related toxicities (herG-1 & II), low drug-likeness scores, and low oral bioavailability. After completing the ADMET search using multiple online servers we found that 55 molecules showed non-toxic behavior. Among the 55 molecules, some molecules have a molecular weight (MW) of more than 500 but not exceeding 700. Furthermore, the drug-likeness of these molecules was assessed, and found three molecules showed higher drug-likeness, and docking hits were found to be higher than the reference molecule (Figure 3, Table S1 & S2).

Toxicity is a major issue in the reported drug molecules (1 to 3 generations) approved by FDA. Currently approved drugs available in the market show multiple complications such as diarrhea, vomiting, skin rashes, and overexpression of EGFR oncogenic target. The erlotinib itself showed hepatotoxicity during prediction in the early stages; hence, alternative medicine is needed to prevent the abnormal and redundant signaling pathways. Further in-silico investigations of three phytochemicals from the database with MW $\leq$ 500 to determine their suitability as EGFR inhibitors.

3.3. Global electrophilicity parameters of lead phytochemicals calculated by the DFT method

The DFT calculations of the best lead phytochemicals Kurarinone, (2S)-2-methoxykurarinone, Sophoraflavanone-G, and erlotinib were done. The calculated values of HOMO, LUMO, electronegativity, hardness, softness, ionization potential, and electron affinity parameters determine the global electrophilicity of the lead molecules and compare them with the reference molecule. The graphical representations of HOMO LUMO and the attained energy band gap (ΔE) in eV are represented in Figure 4a.

The ionization potential (I) directly relates to HOMO energy EHOMO. The regions of HOMO and LUMO were investigated, HOMO orbitals were uniformly distributed over the whole TPSA of molecules and the LUMO was assigned to chromen-6-one among phytochemical Kurarinone, (2S)-2-methoxykurarinone but in Sophoraflavanone G the HOMO orbitals were assigned on the substituted moieties of chromen-6-one and the LUMO shifts were assigned to chromen-6-one. The electronegativity of the reference molecule erlotinib (3.957 eV) matches with the phytochemicals and the values were found to be 3.562 eV, 3.511 eV, and 4.012 eV for Kurarinone, (2S)-2-methoxykurarinone and Sophoraflavanone G respectively (Table 2). These results demonstrated that the reactivity of these phytochemicals is less than that of erlotinib, whereas the stability showed by erlotinib is lower than the stability achieved by the phytochemical lead molecules this envisages that the present selected molecules may show more stability when meets the biological target.

3.4. Analysis of MD simulations

Molecular dynamics simulations are a convenient tool to determine the stability of ligands with the respective target. After screening 1800 phytochemicals, the top docking and higher drug-likeness candidates were assessed for stability and flexibility. Besides these calculations, the Hydrogen bond distance, motions of sampled complexes, Gibbs energy Landscape, compactness of complexes, and protein folding were also calculated. The molecular dynamics simulations were performed for 100 ns. Phytochemicals Kurarinone, (2S)-2-methoxykurarinone, Sophoraflavanone, and erlotinib bound EGFR were subjected to MD Simulations. These phytochemicals are non-toxic as per prediction and share structural identity with reference molecules. Three complexes bound with EGFR and reference-erlotinib bound tyrosine kinase were investigated at the atomistic level.

3.5. Ligand RMSD

The stability of ligand in the binding site of tyrosine kinase was performed and all-lead candidates achieved stability throughout the simulation period. The computed RMSD of the Kurarinone-TKD was found to be 0.25 – 0.45 nm till 78 ns of simulations and then the RMSD increased slightly till the end of simulations. Also, it was observed that the ligand remained in the catalytical site of tyrosine kinase. The

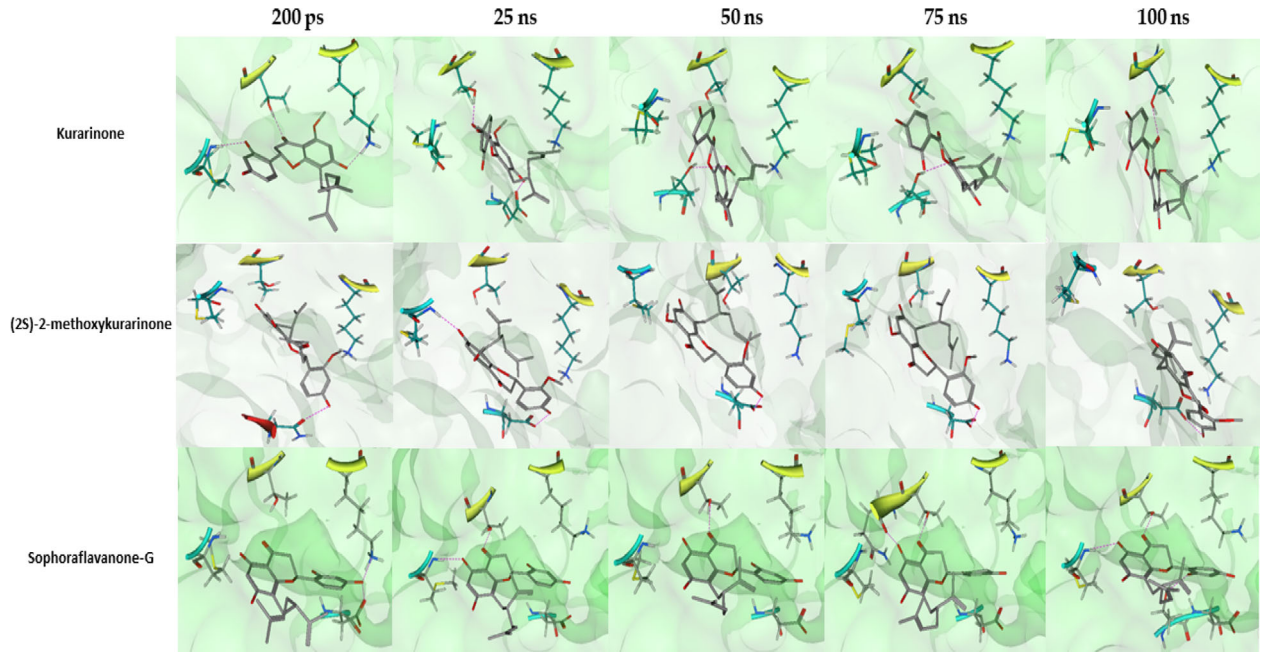

Figure 5. Snapshots of the ligand in the binding site of tyrosine kinase at 200 ps, 25 ns 50 ns, 75 ns, and 100 ns snaps were taken, and analyze the ligand binding pattern also ligand bindings decipher lead molecules remained in the binding site till the simulation is over.

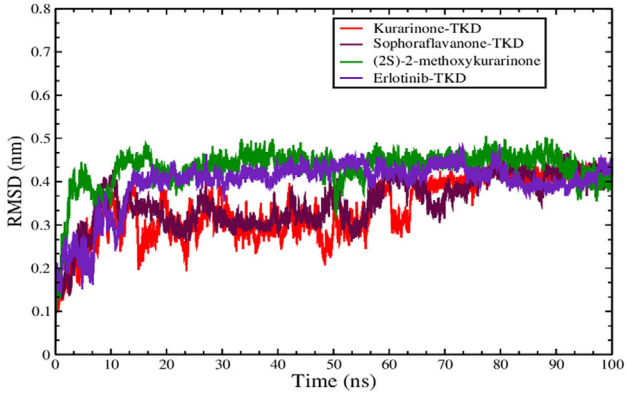

Figure 6. The RMSD Cα of TKD bound with phytochemicals and reference molecules and the color of each complex were annotated and represented in the legend box.

Sophoraflavanone bound TKD attains stability from the very initial step of the simulations and the computed RMSD was found to be 0.3 – 0.5 nm. In complex (2S)-2-methoxykurarinone the computed RMSD was 0.2 – 0.3 nm approximately for the first 12 ns of the simulations then the value remained between 0.3 – 0.4 nm throughout the simulation period also the reference ligand achieved RMSD 0.1 to 0.3 nm till the end of simulation.

The linear RMSD trajectories of ligands reflected from all complexes in this study provide insights into tight bindings with the receptor and thus pave a way for the development of novel phytochemicals (Figure 4b).

The snapshots at different time intervals were taken to analyze the ligand binding pattern and conformations during simulations. It was observed that ligand achieved bindings with the binding site till the end of the simulation period. The interactions were also identified with key amino acids Lys721, Thr766, Gln767, Met769, and Asp830 by each complex (Figure 5).

Kurarinone, (2S)-2-methoxykurarionone, and Sophoraflavanone-G bound with tyrosine kinase showed robust binding with the binding site also conformational changes in ligand Kurarinone were observed after 78 ns of the simulation period. This is because of the conformational change of the ligand that resulted and a slight change in RMSD ranging from 78–100 ns.

3.6. Receptor RMSD

The Cα interconnects all the residues of the protein and thus acts as a major component for the development of protein structure. Higher Cα variability during simulations leads to the deformity of a protein and becomes unstable. Thus, the deformation of protein results in poor structural arrangement. During simulations, the Cα of the TKD bound with the Kurarinone and Sophoraflavanone was computed, and it was found that the Cα attained an equilibrium state when reached 65 to 70 ns and thus attained stability for the rest of the simulation period. Whereas the Cα of the TKD bound with (2S)-2-methoxykurarinone and erlotinib (reference) attained stability from the very initial step till the end of the simulations. Both structures reach the equilibrium at 10 ns of the simulation and achieved stable structural conformations (Figure 6).

3.7. H-bond distance

The Hydrogen bond distance of ligand erlotinib exhibited interactions with Met769 at the hinge region computed by using the gmx_dist module of the gromacs 5.1.1., which provides insights into the ligand bindings and their stability. The Kurarinone does not show interactions with the Met769

Table 3. The average distance and standard deviations of the bonds formed between the ligand and the receptor in the binding site were computed.

Ligand	Bond	Average distance (nm)	Standard deviation (nm)
Kurarinone	UNK-O; Thr766-OG1	0.63403	0.04718
	UNK-O; Lys721-NZ	0.78085	0.06490
	UNK-H; Asp831-OD1	0.85449	0.16072
Sophoraflavanone	UNK-O1; Met769-N	0.54004	0.04528
	UNK-HO4; Asp831-OD1	0.50972	0.06383
	UNK-O3; Thr766-OG1	0.52158	0.05266
	UNK-O2; Thr766-OG1	0.31069	0.04763
(2S)-2-methoxykurarinone	UNK-H5; Arg817-O	0.62692	0.08978
	UNK-H; Thr766-OG	0.96780	0.07762
	UNK-O1; Met-769-N	0.56306	0.08446
Erlotinib	UNK-N2; Met-769-N	0.25031	0.01543

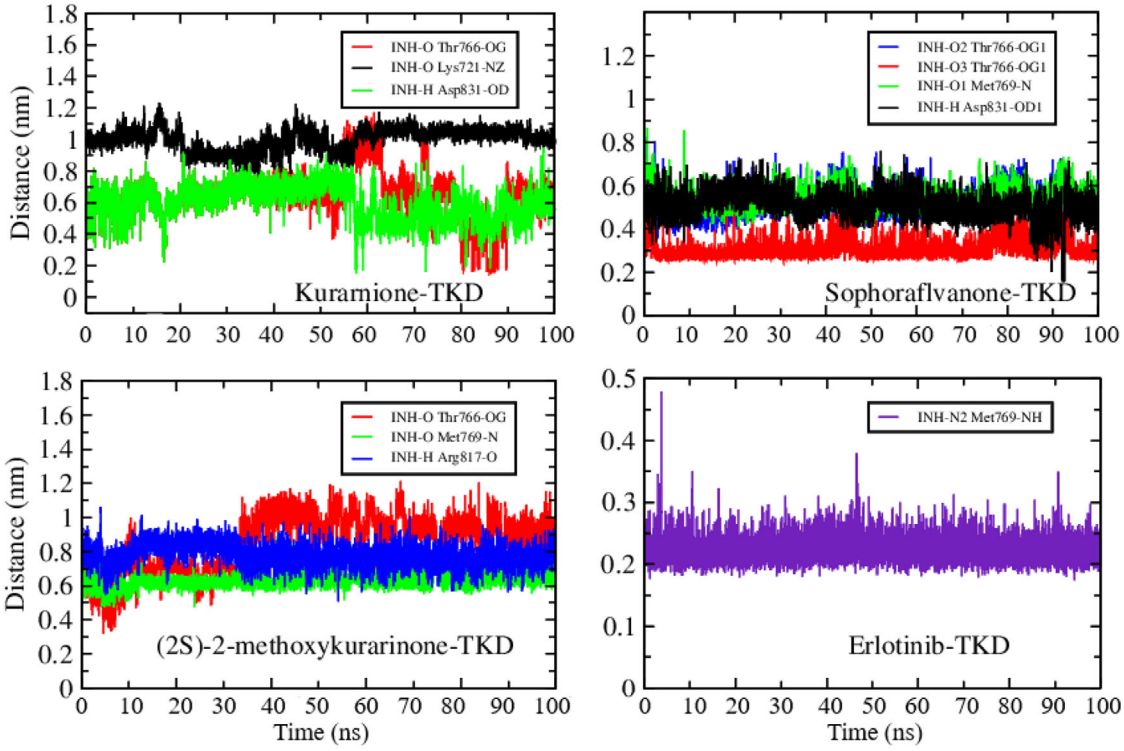

Figure 7. The bond distance trajectories of each complex were computed. All trajectories in each complex were found to be linear.

residue at the hinge region but showed interactions with the binding site. Moreover, the (2S)-2-methoxykurarinone and Sophoraflavanone exhibited interactions with the Met769 at the hinge region and with other key amino acid residues in the binding site. The average distance and standard deviation of the bond formed between the ligand and receptor were also calculated (Table 3). The computed trajectory of the bond distances was given in Figure 7.

3.8. RMSF Analysis of protein

The terminal ends of each phytochemical bound with the TKD were found higher and followed the trend Sophoraflavanone > Kurarinone > (2S)-2-methoxykurarinone > Erlotinib. However, in each complex, the fluctuations in the binding site were lower and values were found to be $0.1 - 0.25$ nm, determined from the below given MD plots. This analysis demonstrated that the ligand binding with the key amino acid residues and the stability of the protein was within permissible limits (Figure 8). This finding is in agreement with the recent published work (Mir et al., 2022)

3.9. Compactness and folding of the TKD bound with phytochemicals

The compactness of the protein during simulations determines the rigidity of the protein computed through the radius of gyrations. The folding of the protein was computed by solvent accessibility surface area which is a driving force on the protein folding. Moreover, both calculations were done using gromacs 5.1.1 software. It was found that compactness in each complex was higher and comparable in each complex bound with phytochemicals as well as erlotinib, except Kurarinone bound TKD showed a gradual increase of the radius of gyrations, determined less compactness of the protein after 90 ns of the simulations which were not too higher (Figure 9).

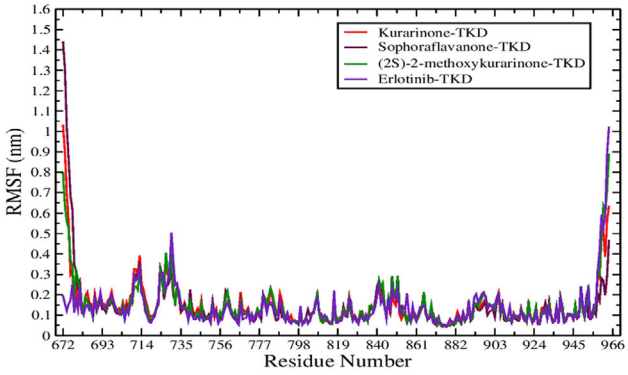

Figure 8. The root mean square fluctuations were computed and the key amino acids show lower fluctuations during simulation in an aqueous medium for a 100 ns time period.

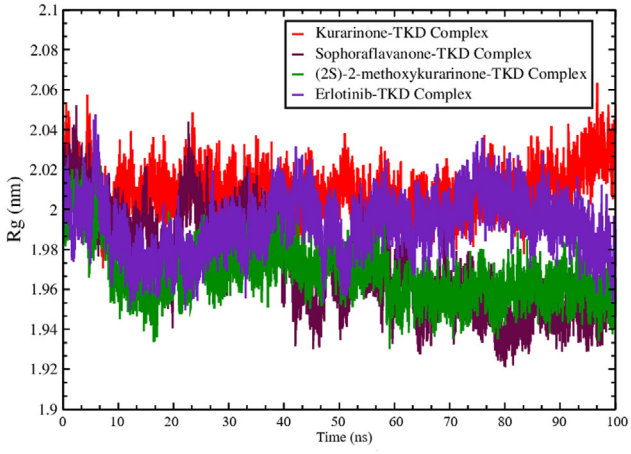

Figure 9. The radius of gyration of the phytochemicals bound with TKD was computed for 100 ns of simulations.

This implied higher compactness resulted in less fluctuations of complexes during simulations in the aqueous medium. The SASA values were found similar in each complex bound with TKD. There were no significant differences when compared with the reference complex. The SASA values ranged between 147.5 and 167.5 nm2 reflected from the obtained trajectories (Figure 10).

3.10. Principal component analysis and Gibbs energy landscape analysis

The flexibility of a protein is commonly determined using essential dynamics. The PCA was used to analyze the protein movements and variations of the simulated TKD bound with the phytochemicals and the reference molecule erlotinib by using backbone Cα dynamics trajectory data. Using gromacs 5.1.1, the eigenvalues and eigenvectors were calculated, using gmx the gmx covar and angien modules, and the principal components were determined (PC1 & PC2).

The difference between the four sampled systems, one reference-bound TKD, and three phytochemicals-bound TKD was shown by the PCA scatter plot created from Cα. Based on the PCA plot, a comparison analysis was conducted. At the C-helix, C-lobe, and N-lobe of the reference-bound TKD complex, compactness was observed in the C-lobe and N-

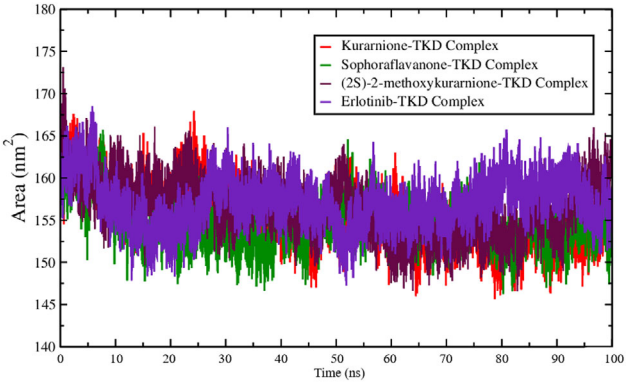

Figure 10. The SASA of the phytochemicals bound with TKD was computed for 100 ns of simulations.

lobe of TKD (Figure 11). This essential dynamic provides insights into the structural conformity of the complexes. Further, the Gibbs energy landscape was done to determine the meta-energy stable states of the complexes. The Gibbs energy landscape was computed for four sampled systems, a reference complex, and three phytochemicals (Kurarinone, Sophoraflavanone, and (2S)-2-methoxykurarinone) bound TKD. The red color indicated the maximum stable conformations state and the blue color denoted the minimum conformational stable energy. The average Gibbs energy landscape of reference bound EGFR-TKD and reference complex was found to be 12 kJ/mol, and (2S)-2-methoxykurarinone bound TKD showed 12.4 kJ/mol (Figure 12). The highest stable conformational state was found in the reference bound TKD which aligns with the (2S)-2-methoxykurarinone bound TKD. The graphical meta-state stable conformations were obtained by using the gmx sham module and gmx xpm2ps was used to generate the quality images. This study demonstrated the reference-bound TKD achieved maximum stability than the other three complexes. But the (2S)-2-methoxykurarinone bound achieved metastable conformations parallel to reference bound TKD.

3.11. Free energy calculations

To compute the average free energy binding of phytochemicals and reference, the last 2000 frames were taken for calculations. The MmPbSaStat.py was used to calculate the binding affinities of ligand-bound receptors. Also, bootstrap analysis was used to determine the average free energy bindings. The free binding energy is a sum of changes in electrostatic energy, van der Waals energy, SASA energy, and polar solvation energy. The average binding free energy of the (2S)-2-methoxykurarinone was found to be -129.555 ± 0.512 kJ/mol and erlotinib exhibited -130.595 ± 0.908 kJ/mol (Table 4). The ΔG binding of (2S)-2-methoxykurarinone aligns with the reference molecule erlotinib. Further, the net contributions of free binding energy by each amino acid residue during simulations were calculated by using the MmPbSaDecomp.py code. The favorable energy contributions by residues of the TKD-bound Sophoraflavanone were found among amino acid residues Val702 = −6.3650, Leu768 = −2.1898, Met729 = −2.2444, and Leu820 = −8.5993 kJ/mol

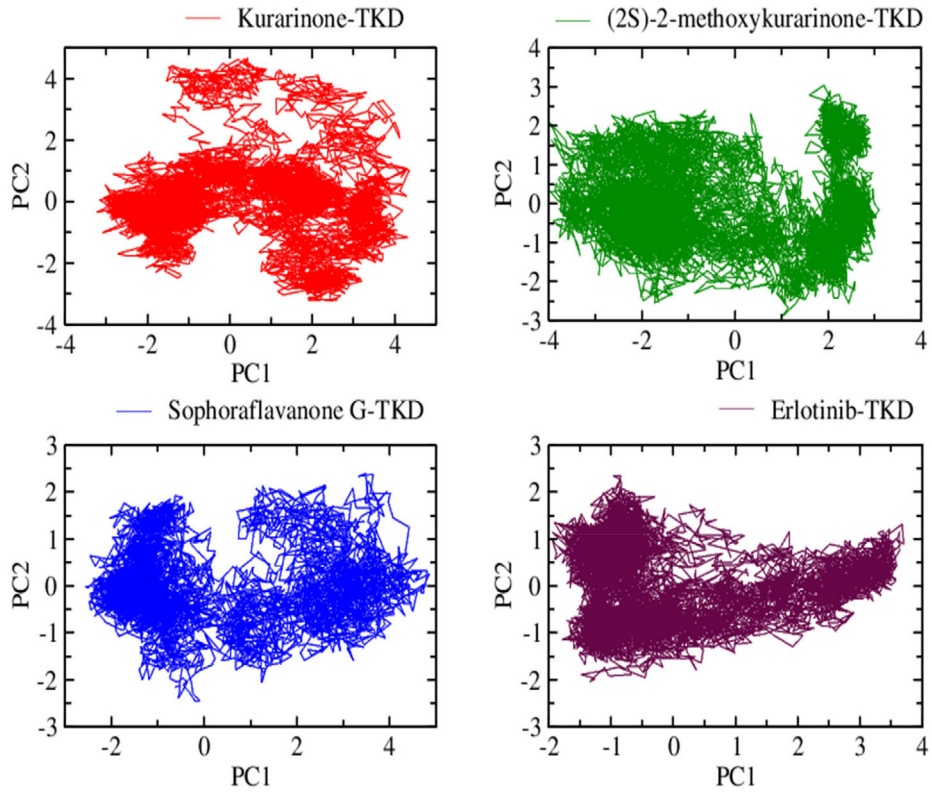

Figure 11. The motion of phytochemical and reference bound TKD were computed by the PCA method using gromacs modules achieved by diagonalizing eigenvalue and eigenvectors and PC1 & PC2 were calculated.

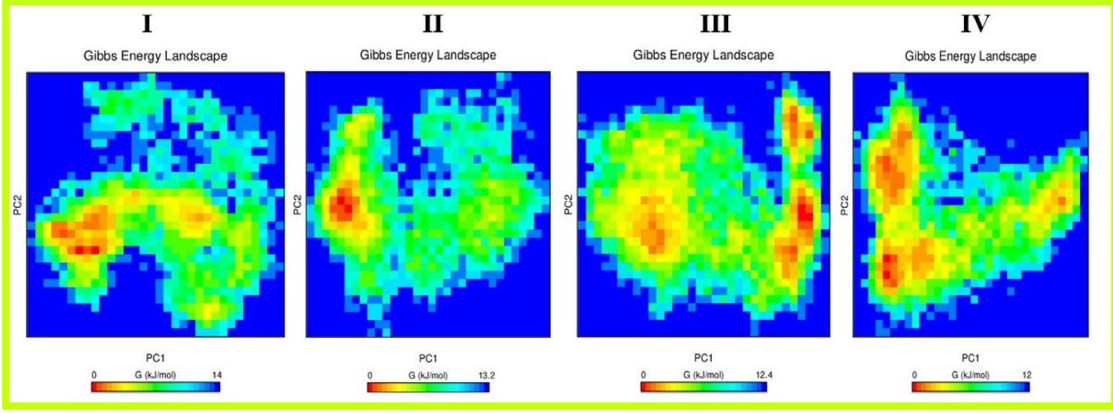

Figure 12. The Gibbs energy landscape of the phytochemicals and reference-bound TKD complexes were represented as (I) Kurarinone (II) Saphoraflavanone (III) (2S)-2-methoxykurarinone and (IV) Erlotinib-TKD complexes showed more conformational stability.

Table 4. Calculated (ΔG) free binding energy of phytochemicals and reference molecule erlotinib along with associated parameters.

	Ligand	ΔEVdW (kJ/mol)	ΔEElec (kJ/mol)	ΔGpolar (kJ/mol)	SASA (kJ/mol)	ΔGbinding (kJ/mol)
1.	Kurarinone	−120.898 ± 1.025	−65.983 ± 1.779	113.557 ± 1.349	−13.865 ± 0.337	−87.170 ± 0.907
2	Sophoraflavanone	−169.033 ± 1.607	−54.877 ± 0.698	165.168 ± 1.794	−18.175 ± 0.171	−76.906 ± 0.787
4	(2S)-2-methoxykurarinone	−177.421 ± 0.480	−42.432 ± 236	105.510 ± 1.081	−15.212 ± 0. 529	−129.555 ± 0.512
4.	Erlotinib	−222.066 ± 0.532	−53.449 ± 0.623	165.597 ± 0.752	−20.680 ± 0.042	−130.595 ± 0.908

and net free energy decomposition contributed by ligand is −54.3916 kJ/mol. (2S)-2-methoxykurarinone bound TKD complex showed favorable net decomposition energy exhibited by amino acids are Val702 = −6.3098, Lys721 = −4.4184, Met769 = −1.5030, Leu820 = −4.5792 and ligand contributes net free energy −72.0803 kJ/mol. Also, the TKD bound Kurarinone complex contributed free energy decomposition via amino acids Leu694 = −2.5847, Phe699 = −4.4156, Val702 = −5.6206, Thr766 = −5.2785, Met769 = −2.7118, Leu820 = −6.9645, Thr830 = −3.5616 and reference complex showed net higher decomposition energy exhibited by amino acid Val702 = −6.7934, Lys721 = −5.1734, Leu768 = − 6.4397,

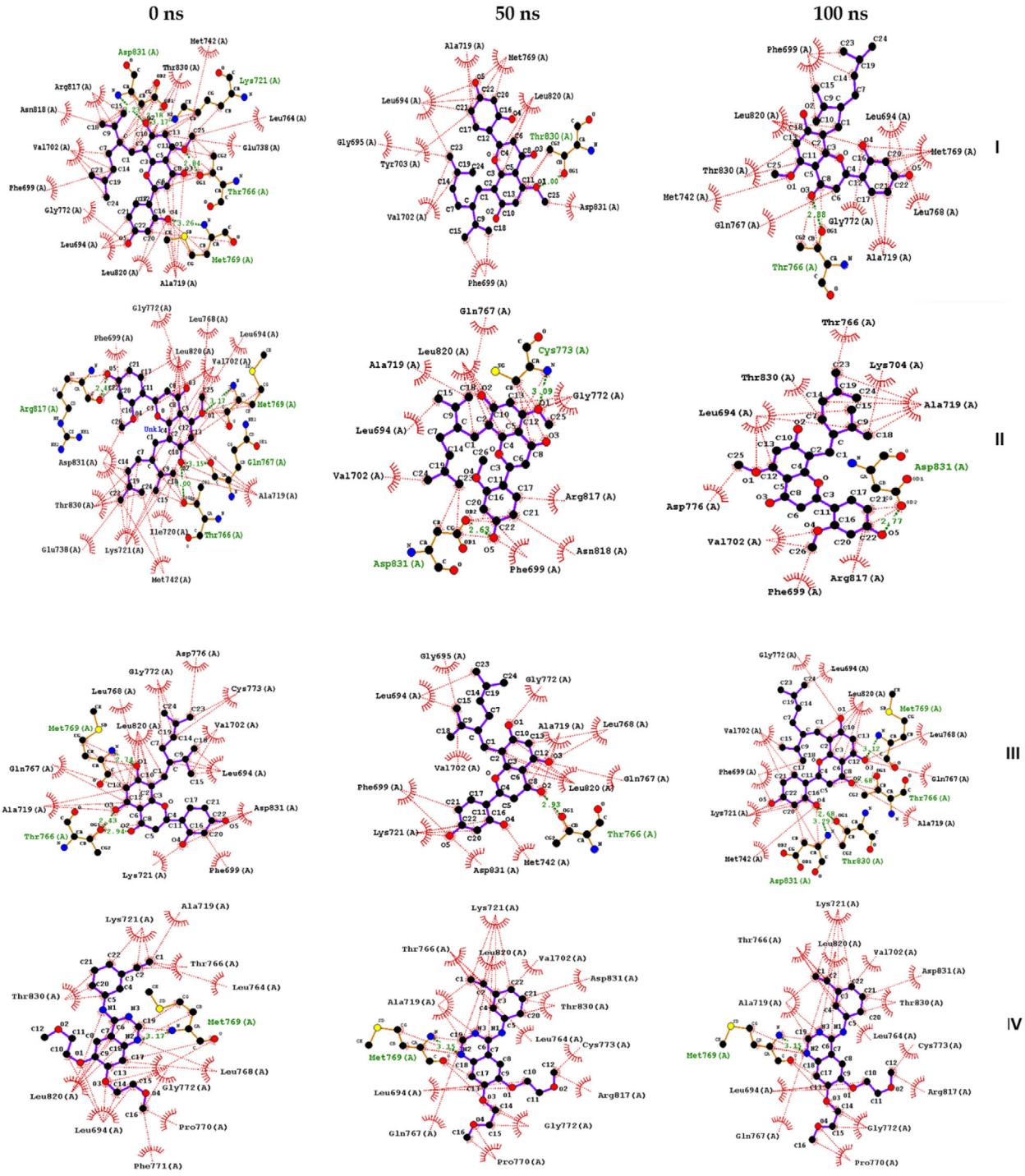

Figure 13. Hydrophobic interactions exhibited by the phytochemicals with the tyrosine is denoted by red dotted lines contacts with amino acids colored in black whereas the amino acids represented in green shows hydrogen bonding with the phytochemicals including control molecule erlotinib. The snapshots were taken at different time intervals (0 ns, 50 ns and 100 ns). The post docking analysis regarding binding of the ligand were explored in detail it was observed the phytochemicals showed hydrogen as well as hydrophobic interactions with the key amino acids in the binding site. Kurarinone, (2S)-2-methoxykurarione, Sophoraflavanone-G and erlotinib are represented in I, II, III, & IV.

Met769 = −2.5473 and Leu820 = −8.5463 and ligand −76.9875 kJ/mol.

3.12. Post docking analysis of ligand bindings with the tyrosine kinase domain (TKD)

We observed the interactions exhibited by the Kurarinone, (2S)-2-methoxykurarione, Sophoraflavanone-G and erlotinib with tyrosine kinase domain at different time intervals to determine the binding pattern of the ligand during simulations. It was found that both the hydrophobic and hydrogen bonding was achieved by the phytochemicals and control molecule erlotinib with TKD. These insights into the ligand bindings and stability with the catalytical site of the TKD and the interactions are given in Figure 13.

4. Conclusion

This study aimed to identify novel phytochemicals from the NPACT database that inhibit redundant tyrosine kinase signaling, which regulates cell metabolism, survival, proliferation, angiogenesis, and motility. We found molecules that follow ADMET properties and are nontoxic. Finally, Kurarinone, (2S)-2-methoxykurarinone, and Sophoraflavanone G phytochemicals showed top docking hits with tyrosine kinase domain and showed higher drug-likeness index. Furthermore, molecular dockings validations of these phytochemicals were done by using molecular dynamics simulations and free binding energy calculations. These computational methods help to determine the movements of selected phytochemicals in the binding pocket and the strength of the bindings. We found phytochemical (2S)-2-methoxykurarinone as a potent molecule that exhibited free binding energy (ΔG binding) comparable to the reference molecule erlotinib. Furthermore, since (2S)-2-methoxykurarinone was used in food supplements, it may be the best choice for inhibiting tyrosine kinase enzyme and the downstream regulating pathways which plays a pivotal role in cellular functions and regulating abnormal cell growth, cell proliferation, angiogenesis, and motility. Further in-vitro and in-vivo studies are essential to determine the efficiency of selected phytochemicals for further validation and clinical trials.

Acknowledgment

Showkat Ahmad Mir wishes to acknowledge DBT-Builder Interdisciplinary Life Sciences Research for providing a fellowship. Showkat Ahmad Mir wishes to acknowledge Dr. Ibrahim Khalifa, assistant professor at Food Tech., Benha University, Egypt, for providing access to MOE09 tools.

Disclosure statement

Authors declare no financial competing interact.

Funding

The author(s) reported there is no funding associated with the work featured in this article.

ORCID

Nirius Jenen Ekka http://orcid.org/0000-0001-7481-761X
Iswar Baitharu http://orcid.org/0000-0002-3046-2076

Authors' contributions

All authors contribute equally

References

Aier, I., Varadwaj, P. K., & Raj, U. (2016). Structural insights into conformational stability of both wild-type and mutant EZH2 receptor. *Scientific reports*, *6*(1) https://doi.org/10.1038/srep34984

Ayoub, A. T., Elrefaiy, M. A., & Arakawa, K. (2019). Computational prediction of the mode of binding of antitumor Lankacidin C to Tubulin. *ACS Omega*, *4*(2), 4461–4471. https://doi.org/10.1021/acsomega.8b03470

Borkotoky, S., & Murali, A. (2018). A computational assessment of pH-dependent differential interaction of T7 lysozyme with T7 RNA polymerase. *BMC Structural Biology*. *17*, 1–11. https://doi.org/10.1186/s12900-017-0077-9

Brooks, B. R., Brooks, C. L., Mackerell, A. D., Nilsson, L., Petrella, R. J., Roux, B., Won, Y., Archontis, G., Bartels, C., Boresch, S., Caflisch, A., Caves, L., Cui, Q., Dinner, A. R., Feig, M., Fischer, S., Gao, J., Hodoscek, M., Im, W., … Karplus, M. (2009). CHARMM: The biomolecular simulation program. *Journal of Computational Chemistry*, *30*(10), 1545–1614. https://doi.org/10.1002/jcc.21287

ACS. (2022). Cancer Facts & Figures. https://www.cancer.org/research/cancer-facts-statistics/all-cancer-facts-figures/cancer-facts-figures-2022.html

Chen, J., Zeng, Q., Wang, W., Sun, H., & Hu, G. (2022). Decoding the identification mechanism of a SAM-III riboswitch on ligands through multiple independent Gaussian-accelerated molecular dynamics simulations. *Journal of Chemical Information and Modeling*, *62*(23), 6118–6132. https://doi.org/10.1021/acs.jcim.2c00961

Chen, J., Zhang, S., Wang, W., Pang, L., Zhang, Q., & Liu, X. (2021). Mutation-induced impacts on the switch transformations of the GDP- and GTP-bound K-Ras: Insights from multiple replica gaussian accelerated molecular dynamics and free energy analysis. *Journal of Chemical Information and Modeling*, *61*(4), 1954–1969. https://doi.org/10.1021/acs.jcim.0c01470

Daina, A., Michielin, O., & Zoete, V. (2017). SwissADME: A free web tool to evaluate pharmacokinetics, drug-likeness and medicinal chemistry friendliness of small molecules. *Scientific reports*, *7*, 42717. https://doi.org/10.1038/srep42717

Ding, P. N., Lord, S. J., Gebski, V., Links, M., Bray, V., Gralla, R. J., Yang, J., C., Lee,., & C., K. (2017). Risk of treatment-related toxicities from EGFR tyrosine kinase inhibitors: A meta-analysis of clinical trials of gefitinib, erlotinib, and afatinib in advanced EGFR-mutated non-small cell lung cancer. *Journal of Thoracic Oncology: Official Publication of the International Association for the Study of Lung Cancer*, *12*(4), 633–643.https://doi.org/10.1016/j.jtho.2016.11.2236

Fantl, W. J., Johnson, D. E., & Williams, L. T. (1993). Signalling by receptor tyrosine kinases. *Annual review of Biochemistry*, *62*(1), 453–481. https://doi.org/10.1146/annurev.bi.62.070193.002321

Garrett, T. P. J., McKern, N. M., Lou, M., Elleman, T. C., Adams, T. E., Lovrecz, G. O., Zhu, H.-J., Walker, F., Frenkel, M. J., Hoyne, P. A., Jorissen, R. N., Nice, E. C., Burgess, A. W., & Ward, C. W. (2002). Crystal structure of a truncated epidermal growth factor receptor extracellular domain bound to transforming growth factor alpha. *Cell*, *110*(6), 763–773. https://doi.org/10.1016/S0092-8674(02)00940-6

Hess, B., Bekker, H., Berendsen, H. J., & Fraaije, J. G. (1997). LINCS: A linear constraint solver for molecular simulations. *Journal of Computational Chemistry*, *18*, 1463–1472. https://doi.org/10.1021/ct5007983

Jeppe Knudsen, S. L., Wai Mac, A. S., Henriksen, L., Deurs, B. V., & Grøvdal, L. M. (2014). EGFR signaling patterns are regulated by its different ligands. *Growth factors (Chur, Switzerland)*, *32*(5), 155–163. Oct 1https://doi.org/10.3109/08977194.2014.952410

Jo, S., Kim, T., Iyer, V. G., & Im, W. (2008). CHARMM-GUI: A web-based graphical user interface for CHARMM. *Journal of Computational Chemistry*, *29*(11), 1859–1865. https://doi.org/10.1002/jcc.20945

Kashefolgheta, S., & Verde, A. V. (2017). Developing force fields when experimental data is sparse: AMBER/GAFF-compatible parameters for inorganic and alkyl oxoanions. *Physical chemistry Chemical Physics : PCCP*, *19*(31), 20593–20607. https://doi.org/10.1039/c7cp02557b

Kumari, R., Kumar, R., & Lynn, A. (2014). g_mmpbsa A GROMACS tool for high-throughput MM-PBSA calculations. *Journal of Chemical Information and Modeling*, *54*(7), 1951–1962. https://doi.org/10.1021/ci500020m

Levin, W. P., Kooy, H., Loeffler, J. S., & Delaney, T. F. (2005). Proton beam therapy. *British journal of Cancer*, *93*(8), 849–854. https://doi.org/10.1038/sj.bjc.6602754

Lindorff-Larsen, K., Piana, S., Palmo, K., Maragakis, P., Klepeis, J. L., Dror, R. O., & Shaw, D. E. (2010). Improved side-chain torsion potentials for

the Amber ff99SB protein force field. *Proteins*, *78*(8), 1950–1958. https://doi.org/10.1002/prot.22711

Mebi, C. A. (2011). DFT study on structure, electronic properties, and reactivity of cis-isomers of [(NC 5 H 4-S) 2 Fe (CO) 2]. *Journal of Chemical Sciences*, *123*(5), 727–731. https://doi.org/10.1007/s12039-011-0131-2

Melosky, B., & Hirsh, V. (2014). Management of common toxicities in metastatic NSCLC related to anti-lung cancer therapies with EGFR–TKIs. *Frontiers in Oncology*, *4*, 238. https://doi.org/10.3389/fonc.2014.00238

Mir, S. A., Dash, G. C., Meher, R. K., Mohanta, P. P., Chopdar, K. S., Mohapatra, P. K., Baitharu, I., Behera, A. K., Raval, M. K., & Nayak, B. (2022). In Silico and In Vitro Evaluations of Fluorophoric Thiazolo-[2, 3-b] quinazolinones as Anti-cancer Agents Targeting EGFR-TKD. *Applied Biochemistry and Biotechnology*, *194*, 4298-4318. https://doi.org/10.1007/s12010-022-03893-w

Mir, S. A., & Nayak, B. (2022). Exploring binding stability of hydroxy-3-(4-hydroxyphenyl)-5-(4-nitrophenyl)-5, 5a, 7, 8, 9, 9a-hexahydrothiazolo [2, 3-b] quinazolin-6-one with T790M/L858R EGFR-TKD. *Journal of Biomolecular Structure and Dynamics*, 1–15. https://doi.org/10.1080/07391102.2022.2053748

Molsoft, L. L. C. (2007). 3366, North Torrey Pines Court, Suite 300, La Jolla, CA 92037, USA.

Mori, Y., Kida, Y., Matsushita, Y., Mizumatsu, S., & Hatano, M. (2020). Stereotactic radiosurgery and stereotactic radiotherapy for malignant skull base tumors. *Cureus*, *12*(6), 1-10. https://doi.org/10.7759/cureus.8401

Muhammad, A., Khunrae, P., & Sutthibutpong, T. (2020). Effects of oligolignol sizes and binding modes on a GH11 xylanase inhibition revealed by molecular modeling techniques. *Journal of Molecular Modeling*, *26*(6), 124. https://doi.org/10.1007/s00894-020-04383-8

O'Boyle, N. M., Banck, M., James, C. A., Morley, C., Vandermeersch, T., & Hutchison, G. R. (2011). Open Babel: An open chemical toolbox. *Journal of Cheminformatics*, *3*(1), 1–14.

Ogiso, H., Ishitani, R., Nureki, O., Fukai, S., Yamanaka, M., Kim, J.-H., Saito, K., Sakamoto, A., Inoue, M., Shirouzu, M., & Yokoyama, S. (2002). Crystal structure of the complex of human epidermal growth factor and receptor extracellular domains. *Cell*, *110*(6), 775–787. https://doi.org/10.1016/S0092-8674(02)00963-7

Oliveira, M. (2015). Managing common toxicities with new tyrosine kinase inhibitors. *CancerWorld*, *69*, 31–37.

Parr, R. G., Szentpály, L. V., & Liu, S. (1999). Electrophilicity index. *Journal of the American Chemical Society*, *121*(9), 1922–1924. https://doi.org/10.1021/ja983494x

Pereira, G. R. C., Da Silva, A. N. R., Do Nascimento, S. S., & De Mesquita, J. F. (2019). In silico analysis and molecular dynamics simulation of human superoxide dismutase 3 (SOD3) genetic variants. *Journal of Cellular Biochemistry*, *120*(3), 3583–3598. https://doi.org/10.1002/jcb.27636

Pires, D. E., Blundell, T. L., & Ascher, D. B. (2015). pkCSM: Predicting small-molecule pharmacokinetic and toxicity properties using graph-based signatures. *Journal of Medicinal Chemistry*, *9*, 4066–4072. https://doi.org/10.1021/acs.jmedchem.5b00104

Pye, S. M., Cortes, J., Ault, P., Hatfield, A., Kantarjian, H., Pilot, R., Rosti, G., & Apperley, J. F. (2008). The effects of imatinib on pregnancy outcome. *Blood*, *111*(12), 5505–5508. https://doi.org/10.1182/blood-2007-10-114900

Sakata, Y., Kawamura, K., Shingu, N., Hiroshige, S., Yasuda, Y., Eguchi, Y., Anan, K., Hisanaga, J., Nitawaki, T., Nakano, A., et al. (2020). The effects of switching EGFR-TKI treatments for non-small cell lung cancer because of adverse events. *Asia-Pacific Journal of Clinical Oncology*, *16*(2), e113-e117. https://doi.org/10.1111/ajco.13103

Shah, R. R., & Shah, D. R. (2019). Safety and tolerability of epidermal growth factor receptor (EGFR) tyrosine kinase inhibitors in oncology. *Drug safety*, *42*(2), 181–198.https://doi.org/10.1007/s40264-018-0772-x

Shimizu, M., Adachi, S., Masuda, M., Kozawa, O., & Moriwaki, H. (2011). Cancer chemoprevention with green tea catechins by targeting receptor tyrosine kinases. *Molecular nutrition & Food Research*, *55*(6), 832–843. https://doi.org/10.1002/mnfr.201000622

Shimizu, M., Shirakami, Y., & Moriwaki, H. (2008). Targeting receptor tyrosine kinases for chemoprevention by green tea catechin, EGCG. *International journal of Molecular Sciences*, *9*(6), 1034–1049. https://doi.org/10.3390/ijms9061034

Sousa da Silva, A. W., & Vranken, W. F. (2012). ACPYPE-Antechamber python parser interface. *BMC research Notes*, *5*, 1–8. https://doi.org/10.1186/1756-0500-5-367

Stamos, J., Sliwkowski, M. X., & Eigenbrot, C. (2002). Structure of the epidermal growth factor receptor kinase domain alone and in complex with a 4-anilinoquinazoline inhibitor. *Journal of Biological Chemistry*, *48*, 46265–46272. https://doi.org/10.1074/jbc.M207135200

Wang, J., Wang, W., Kollman, P. A., & Case, D. A. (2006). Automatic atom type and bond type perception in molecular mechanical calculations. *Journal of Molecular Graphics & Modelling*, *25*(2), 247–260. https://doi.org/10.1016/j.jmgm.2005.12.005

Wang, J., Youkharibache, P., Zhang, D., Lanczycki, C. J., Geer, R. C., Madej, T., Phan, L., Ward, M., Lu, S., Marchler, G. H., Wang, Y., Bryant, S. H., Geer, L. Y., & Marchler-Bauer, A. (2020). iCn3D, a web-based 3D viewer for sharing 1D/2D/3D representations of biomolecular structures. *Bioinformatics (Oxford, England)*, *36*(1), 131–135. https://doi.org/10.1093/bioinformatics/btz502

Xia, H., Dai, X., Yu, H., Zhou, S., Fan, Z., Wei, G., Tang, Q., Gong, Q., & Bi, F. (2018). EGFR-PI3K-PDK1 pathway regulates YAP signaling in hepatocellular carcinoma: the mechanism and its implications in targeted therapy. *Cell death & Disease*, *9*(3), 1–2. https://doi.org/10.1038/s41419-018-0302-x

Xu, D., Li, G., Li, H., & Jia, F. (2017). Comparison of IMRT versus 3D-CRT in the treatment of esophagus cancer: A systematic review and meta-analysis. *Medicine*, *96*, 31. https://doi.org/10.1097/MD.0000000000007685

Yang, T., Wu, J. C., Yan, C., Wang, Y., Luo, R., Gonzales, M. B., Dalby, K. N., & Ren, P. (2011). Virtual screening using molecular simulations. *Proteins*, *79*(6), 1940–1951. https://doi.org/10.1002/prot.23018